

Prediction of Specific Biomolecule Adsorption on Silica Surfaces as a Function of pH and Particle Size

By

Fateme S. Emami[†], Valeria Puddu[‡], Rajiv J. Berry[§], Vikas Varshney[§], Siddharth V. Patwardhan^{||},
Carole C. Perry^{†*}, and Hendrik Heinz^{†*}

[†] Department of Polymer Engineering, University of Akron, Akron, Ohio 44325-0301, USA

[‡] Interdisciplinary Biomedical Research Centre, School of Science and Technology, Nottingham
Trent University, Clifton Lane, Nottingham NG11 8NS, UK

[§] Materials and Manufacturing Directorate, Air Force Research Laboratory, Wright-Patterson Air
Force Base, Ohio 45433, USA

^{||} Department of Chemical and Process Engineering, University of Strathclyde, 75 Montrose
Street, Glasgow G1 1XJ, UK

* Corresponding authors: carole.perry@ntu.ac.uk, hendrik.heinz@uakron.edu

Abstract

Silica nanostructures are biologically available and find wide applications for drug delivery, catalysts, separation processes, and composites. However, specific adsorption of biomolecules on silica surfaces and control in biomimetic synthesis remain largely unpredictable. In this contribution, the variability and control of peptide adsorption on silica nanoparticle surfaces is explained as a function of pH, particle diameter, and peptide electrostatic charge using molecular dynamics simulations with the CHARMM-INTERFACE force field. Adsorption free energies and specific binding residues are analyzed in molecular detail, providing experimentally elusive, atomic-level information on the complex dynamics of aqueous electric double layers in contact with biological molecules. Tunable contributions to adsorption are described in the context of specific silica surface chemistry, including ion pairing, hydrogen bonds, hydrophobic interactions, and conformation effects. Remarkable agreement is found for computed peptide binding as a function of pH and particle size versus experimental adsorption isotherms and zeta-potentials. Representative surface models were built using characterization of the silica surfaces by TEM, SEM, BET, TGA, ζ -potential, and surface titration measurements. The results show that the recently introduced interatomic potentials (Emami et al. Chem. Mater. 2014, 26, 2647) enable computational screening of a limitless number of silica interfaces to predict the binding of drugs, cell receptors, polymers, surfactants, and gases under realistic solution conditions at the scale of 1 to 100 nm. The highly specific binding outcomes underline the significance of the surface chemistry, pH, and topography.

1. Introduction

Silicon dioxide, or silica, is widely available in mineral form, biologically enriched in organisms, and produced by laboratory synthesis.¹⁻³ It is extensively used as a filler material in nanocomposites and tires, in separation media for liquids and gases, cosmetics, catalyst supports, and building materials. Porous silica nanoparticles that exploit specific interactions with biological molecules in aqueous solution are also used in drug delivery systems, biomarkers, sensors, and nano-reactors.⁴⁻¹⁰ The performance for this broad range of applications is often still evaluated by trial and error and results remain difficult to explain. For example, efforts to synthesize silica from precursors to replicate hierarchically organized silica-protein skeletons similar to diatoms, marine organisms,^{5, 11, 12} and plants have shown first successes in achievable structural order.^{7, 9, 13-17} However, fundamental insight into mechanisms and control of assembly remains incomplete even though many amino acid sequences, peptides and proteins from microorganisms, cellular templates, and designed ligands were tested.^{6-10, 14, 18}

Therefore, better understanding of the role of the precursors, of the surface chemistry of silica formed, as well as of the competitive interactions with solvents and proteins could provide significant benefits to the rational engineering of silica-based materials. The effect of synthesis conditions, pH, buffer composition, and molecular conformation on materials formation is known to be critical.^{9, 19, 20} However, limitations of current laboratory instrumentation pose difficulties to answer questions related to silica biomineralization and specific molecular recognition at the scale of 1 to 100 nm while complementary guidance from simulations can be very helpful.^{9, 18, 21-36}

Studies by biopanning and molecular simulation with the polymer consistent force field (PCFF) extended to silica recently identified a range of contributions to specific adsorption of

peptides on amorphous silica particles.^{9, 10,26} These contributions include ion pairing between positively charged groups in the peptides and siloxide groups on the silica surface accompanied by neutralization of the ζ -potential, hydrogen bonds, van-der-Waals interactions with the surface, and conformation effects. The significance of each of these adsorption modes was found to depend on experimental conditions such as pH, peptide sequence, and silica surface chemistry. As a consequence, the nature and strength of the interactions can only be identified using dedicated molecular models that represent closely the experimental conditions.

The aim of this contribution is the atomic-scale visualization of the binding process and *quantitative* predictions of specific adsorption of peptides to all types of silica surfaces using computer simulations. A companion paper recently introduced accurate force field parameters and a detailed surface model database for silica,³⁷ which are employed here in the form of the CHARMM-INTERFACE force field.²⁶ This study focuses on the effects of pH and particle size that modulate ionization, surface structure, and specific peptide adsorption (Figure 1).^{9, 38-41} The chosen peptides include consensus silica binding sequences composed of seven amino acids with different net charge (-1, 0, +1) and hydrophilicity that were previously identified by phage display (Table 1).¹⁰ The chosen nanoparticles are of diameters 28 nm, 82, nm, and 210 nm, and have undergone characterization of their surface chemistry by BET, BJH, TGA, TEM, SEM, and ζ -potential measurements (Figure 1).⁴²

The outline of this paper is as follows. The recently introduced force field and surface model database for silica interfaces are briefly reviewed (section 2). Specific peptide adsorption, binding free energies, and mechanisms of interaction with silica surfaces are described as a function of pH and particle size, illustrating predictive details from simulation (section 3). A summary of the major results and conclusions follows at the end (section 4). The Supporting

Information provides full details of computational and experimental methods, experimental data employed for validation, as well as further information (sections S1 to S4).

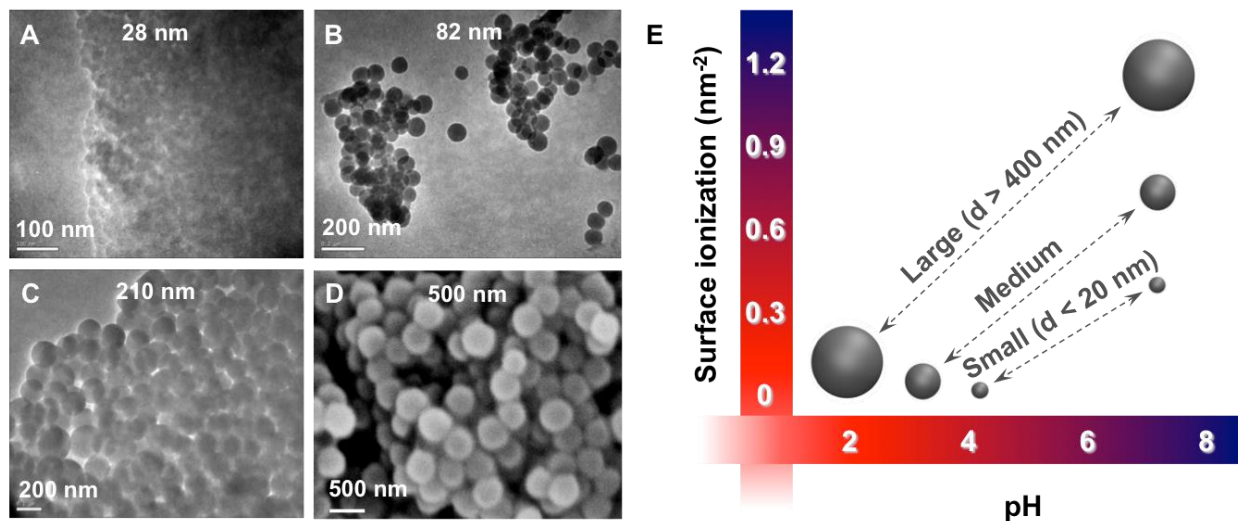


Figure 1. Electron microscopy images of amorphous silica nanoparticles of different size from Stöber-type synthesis, and the effect of pH and particle size on surface ionization (from refs. ^{42,37}). (A-D) TEM and SEM images for nanoparticles of average sizes 28, 82, 210, and 500 nm (ref. ⁴²). Silica nanoparticles of size 28 nm are less dense and poorly defined in comparison to spherical larger particles. (E) Schematic relationship between surface ionization, pH, and particle size. Large nanoparticles contain Q²/Q³ surface environments, medium size and smaller nanoparticles contain mostly Q³ environments. The amount of SiO⁻Na⁺ groups per nm² is shown at an ionic strength of 0.1-0.3 mol·dm⁻³ (see further details in Table S1 and original data in refs. ^{9, 38-41}).

Table 1. Sequence, charge, isoelectric point, and hydrophilicity of the selected peptides, identified by phage display.¹⁰

Peptide name	Sequence	Net charge at pH=7.4	pI ^a	Hydrophilicity ^a
S1	K ⁺ LPGWSG · Cl ⁻	+1	9.8±0.2	-0.3
S2	AFILPTG	0	5.8±0.2	-1
S3	LD ⁻ HSLHS · Na ⁺	-1	6.1±0.1	-0.1

^a Values close to zero correspond to hydrophilicity and values close to -1 hydrophobicity. Calculated according to ref. ⁴².

2. Recent Developments in Modeling and Simulation of Silica Interfaces

A companion paper introduced a force field and a surface model database for silica to simulate bulk, surface, and interfacial properties in atomic resolution.³⁷ This work discusses chemical bonding and surface features of silica in depth to enable quantitative studies of silica-biomolecular interfaces at the scale of 1 nm to 100 nm under realistic solution conditions. Major improvements in the force field include the chemically consistent representation of ionic versus covalent bonding in silica, incorporation of full details of surface chemistry, surface ionization, as well as validation of interfacial properties in ~5% agreement with experiment, down from up to 500% error previously. Prior force fields often required fixed atoms to avoid collapse of the models in the simulation, neglected the pH dependence of the surface chemistry, and involved other drastic approximations so that even approximate predictions of specific binding of biomolecules were essentially impossible.⁴³⁻⁵⁶

The new, thermodynamically consistent silica parameters are compatible with comprehensive harmonic force fields for biopolymers, organic molecules, and inorganic compounds such as

CHARMM, AMBER, PCFF, COMPASS, CVFF, and INTERFACE.^{26, 37} The compatibility enables insight into a limitless number of silica hybrid materials by the possible combination of thousands of distinct silica surface structures with billions of distinct biopolymers, surfactants, and receptor molecules across a wide range of concentrations and solution conditions. A surface model database covers experimentally observed surface chemistries of all types of silica and aids in the preparation of customized nanostructures for given conditions (Table S1).³⁷

The novel features of the force field and of the surface model database are summarized more inclusively as follows: (1) full atom mobility, (2) reproduction of the lattice parameters of crystalline silica, (3) coverage of the full range of surface chemistry with Q², Q³, Q⁴, amorphous, and porous environments, (4) coverage of the full range of surface ionization corresponding to surface type and pH, (5) agreement of computed immersion energies, contact angles of water, and adsorption isotherms with laboratory measurements (using common SPC and TIP3P water models), (6) correlation of cation dissociation with measured ζ -potentials as a function of pH and nanoparticle size, (7) full compatibility with many harmonic energy expressions (see above). These features are described in ref. ³⁷. The present contribution illustrates that the accurate reproduction of the structure and interfacial properties of pristine silica provides a solid foundation for realistic simulations of complex silica-organic and silica-biomolecular interfaces. The improvements in accuracy up to two orders of magnitude over earlier models^{9, 32, 53, 57-64} result from the precise implementation of chemical details in the INTERFACE force field,²⁶ as also shown for other inorganic-organic interfaces.^{9, 21, 25, 29, 30, 65-72}

3. Results and Discussion

3.1. Specific Peptide Adsorption as a Function of pH. The three peptides shown in Table 1 and silica nanoparticles of 82 nm uniform size (Figure 1b) were chosen to investigate the impact of pH on specific peptide adsorption. Extensive experimental characterization of the silica surfaces by BET, TGA, and ζ -potential measurements as well as of peptide adsorption by adsorption isotherms is available (Figures S1 to S3).^{10, 42} The nanoparticle surfaces at pH values of 3, 5, 7.4, and 8.5 were represented by regular Q³ silica surfaces with specific degrees of ionization of silanol groups $\equiv\text{Si-OH}$ to siloxide groups $\equiv\text{SiO}^- \cdots \text{Na}^+$ (Figure 2).¹⁰ The degrees of ionization are 0%, 9%, 18%, and 50%, respectively (see details in Table S1).³⁷ The chemical appearance of these surfaces differs significantly, leading to an amount of dissociated cations of 0, 0.27, 0.45, and 0.30 cations per nm², whereby the value of 50% silanol ionization corresponds to maximum ionization of the silica surface somewhat above pH 8.5.³⁷ The pH values of the peptides were represented by the appropriate charge state of pH-sensitive residues (N-terminus, K, D, H, N-terminus) and addition of oppositely charged ions to maintain overall charge neutrality when needed (Na^+ , Cl^-).

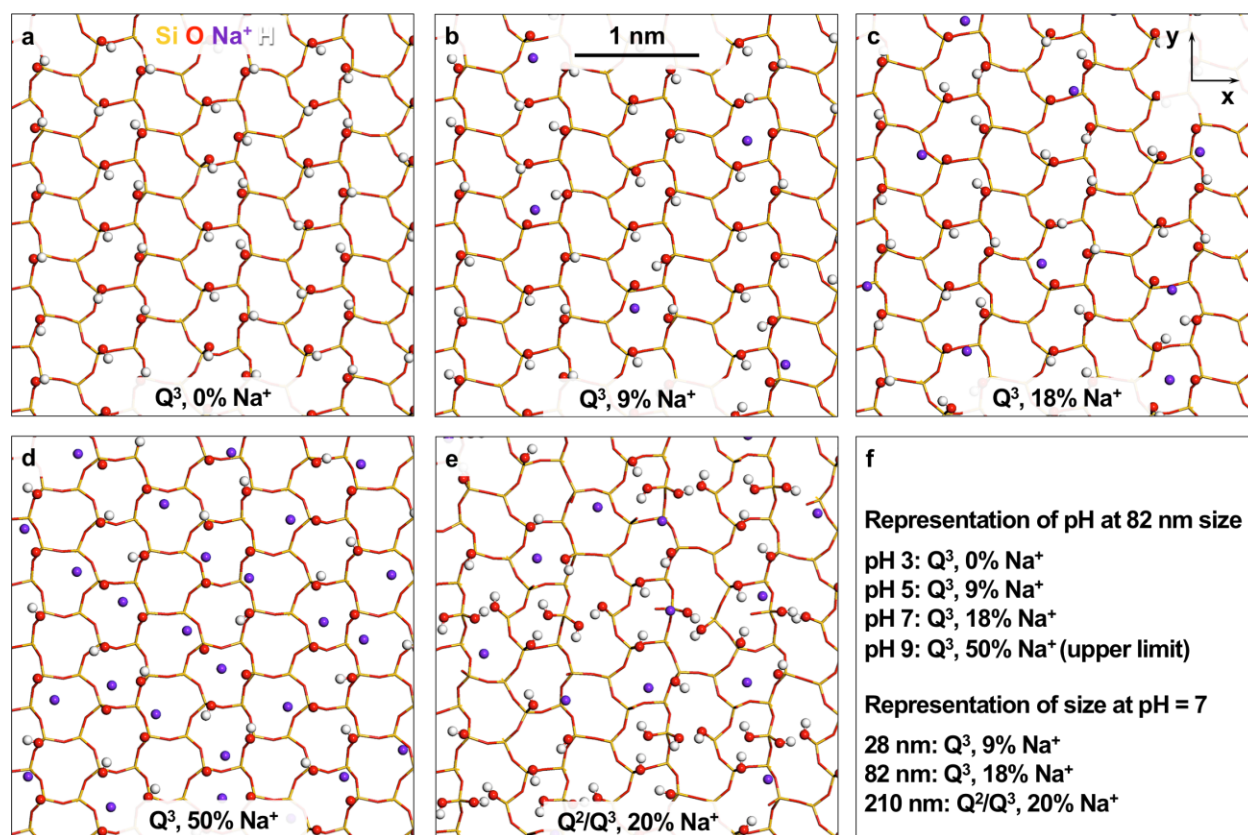


Figure 2. Silica model surfaces for different pH and particles of different size in top view. (a-d) Regular Q³ surfaces with 4.7 SiO(H, Na) groups per nm² and different amount of SiO⁻Na⁺ groups represent pH values of 3, 5, 7, and 9 for 82 nm size nanoparticles. (e) The regular Q²/Q³ surface with 6.5 SiO(H, Na) groups per nm² and 20% ionization represents 210 nm size particles at pH 7. High area density of both SiOH and of SiO⁻Na⁺ groups results in stronger adsorption of all peptides. Models for particles of 28 nm and 82 nm size at pH 7 correspond to (b) and (c). (f) Summary of correspondence of chosen models to pH and particle size near physiological ionic strength.

Large-scale parallel molecular dynamics simulations of the three peptides on the silica surfaces were then carried out, including multiple independent start conformations, thermal annealing, and total simulations times in excess of 20 ns (Figures 3 and 4, see details in section

S1).⁷³ A very good correlation between the amount of adsorbed peptides in the adsorption isotherm (Figure 3a)¹⁰ and the percentage of time close to the surface in the simulations was observed (Figure 3b) without any further assumptions. Close contact of the peptides was thereby defined as a distance of less than 3 Å from the surface oxygen atoms. Computed adsorption energies DE_C and computed adsorption free energies ΔF_C also correlate with the adsorbed amount of peptide in experiment (Table 2). Values further below zero correspond to attraction and a larger amount adsorbed. Nearly equal values of adsorption energies and adsorption free energies are notable, whereby computed adsorption free energies are shown only for the cationic peptide KLPGWSG due to the high computational cost of umbrella sampling and steered MD (Table 2 and section S1). Using the relation $\Delta F_C = DE_C - T\Delta S_C$, it is found that net entropic contributions to adsorption $-T\Delta S_C$ are small, essentially within the uncertainty of ± 2 kcal/mol. Therefore, the adsorption energy DE_C is a good first approximation for the free energy of binding ΔF_C of short peptides. Similar suggestions were made earlier for the binding of peptides on metal and silica surfaces in aqueous solution.^{9,22, 67, 73} The present quantitative data therefore confirm a certain entropy loss of the peptide upon adsorption due to decreased conformational freedom, which is compensated, or slightly overcompensated, by the release of surface-bound water that gains translational and rotational mobility. Computed binding free energies ΔF_C of 0, -1, -6, and -8 kcal/mol (± 0.5 kcal/mol) on 0%, 9%, 18%, and 50% ionized surfaces also agree with binding free energies ΔF_A in a range -4 to -7 kcal/mol for peptide KLPGWSG derived from the adsorption isotherms (Table S2). The experimental values ΔF_A were derived from approximate binding constants K_A according to $\Delta F_A = -RT \ln K_A$, and uncertainties are also difficult to reduce below ± 2 kcal/mol (section S1.4).¹⁰ In addition, computed adsorption energies

correlate with the experimental threshold concentration of peptides to achieve significant adsorption (section S3).

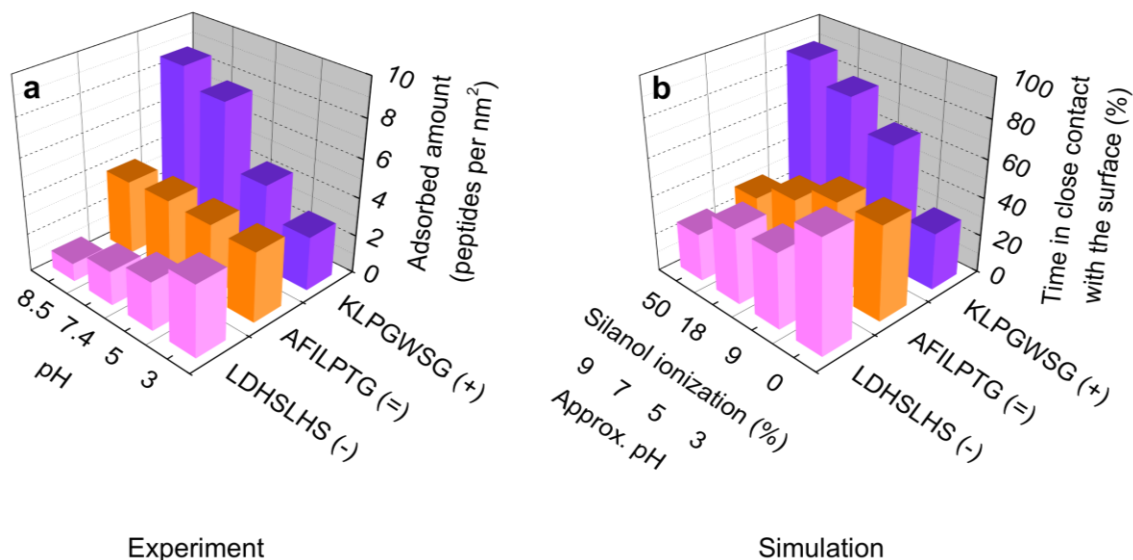


Figure 3. Peptide adsorption on silica nanoparticles of average diameter 82 nm with 4.7 silanol groups per nm² as a function of pH by measurement and simulation. (a) Adsorbed amount of three peptides of different charge as a function of pH at 1 mM initial concentration (from ref. ¹⁰). (b) Percentage of time the same peptides spend in close contact with Q³ silica surfaces of different ionization according to simulation (<3 Å). Different pH states of the surface are embodied in the model by differences in silanol ionization.

Table 2. Computed energy of adsorption of the peptides on Q³ silica surfaces of different pH value according to molecular dynamics simulation (± 2 kcal/mol). Computed free energies of adsorption are also shown for KPLGWSG (± 0.5 kcal/mol).

Peptide (charge at pH 7)	Adsorption energy (kcal/mol)			
	pH~3	pH~5	pH~7.4	pH>8.5
	(0% ionized)	(9% ionized)	(18% ionized)	(50% ionized)
KLPGWSG (+)	-1	-1	-3	-7
KLPGWSG (+) - Free energy	0	-1	-6	-8
AFILPTG (=)	+3	+1	+3	+4
LDHSLHS (-)	-2	+1	+2	+4

A major benefit from the simulation is access to structural information on the atomic scale (Figure 4 and Table 3). Visualizations (Figure 4) and time-averaged information on the proximity of individual residues and residence times on the surface (Table 3) explain the mechanism of selective adsorption. The positively charged peptide KLPGWSG is more attracted to surfaces at higher pH that carry an increased negative charge per area (Figure 3). On the 50% and 18% ionized surfaces, i.e., at pH 9 and 7, the peptide is anchored to the surface by the ammonium groups of the N-terminal and the K1 side chain for more than 80% of the time (Figure 4a). At lower ionization of 9% and 0%, i.e. at pH 5 and 3, electrostatic interactions through ion pairing are diminished and hydrogen bonds of the OH groups of S6 and of ammonium groups on N-terminal K1 with the silica surface increasingly contribute to adsorption (Figure 4b, c). In addition, close contacts of L2, P3, and W5 side chains with the surface are seen (Table 3). Hydrophobic residues have thereby no intrinsic affinity to the silica surface; their

surface attachment mainly diminishes disruptions of the hydrogen-bonded structure of liquid water. Near-neutral silica surfaces therefore attract hydrophobic residues to concentrate unfavorable hydrophobic (van-der-Waals) interactions directly at the surface, however, hydration shells of siloxide ions and cations keep hydrophobic residues away on ionized silica surfaces. The time-averaged adsorbed conformation of the positively charged peptide KLPGWSG, therefore, changes from anchor-like with strong contribution by ammonium groups on highly negatively charged surfaces (Figure 4a) to flat-on arrangements with higher mobility (Figure 4c) and more contact of polar and hydrophobic functional groups on the less ionized surfaces (L2, P3, W5).

Adsorption of the overall neutral peptide AFILPTG was weaker than for KLPGWSG and statistically not affected by changes in surface ionization and pH (Figure 3). Interactions with the 50% ionized surface, which exceed the experimental surface charge, were found to be slightly more repulsive than in experiment (Table 3). On all other surfaces, the peptide was in contact with the silica surface at least 40% of the simulation time through the N-terminal ammonium group by electrostatic forces (ion pairing) as well as through hydrogen bonds that involve the carboxylate of the C-terminal and the OH group in T6 in contact with surface silanol groups (Figure 4d). Additional hydrophobic interactions were observed through the phenyl ring in F2, the L4 side chain, and the ring of P5 in agreement with experimental observations (Figure 4e and Table 3).¹⁰

The negatively charged peptide LDHSLHS showed less time in contact with most surfaces than the other two peptides and adsorption decreased with higher density of negative charge (Figure 3, Table 3). This peptide also notably changes its own charge from approximately -1.5 at pH 8.5 to +2 at pH 3.⁴² Direct contact with the highly ionized surface at pH 8.5 amounted to

only 20% of simulation time (Figure 4f) and increased to above 40% of simulation time for 18% and 9% ionized silica surfaces respectively (Figure 4g). The N-terminus of L1 and hydroxyl groups in S7, as well as some hydrophobic groups approach the surface at lower pH (Table 3). At the point of zero charge, the peptide is in close contact with the surface for more than 60% of simulation time, including protonated H3, H6, and temporarily all residues (Figure 4h).

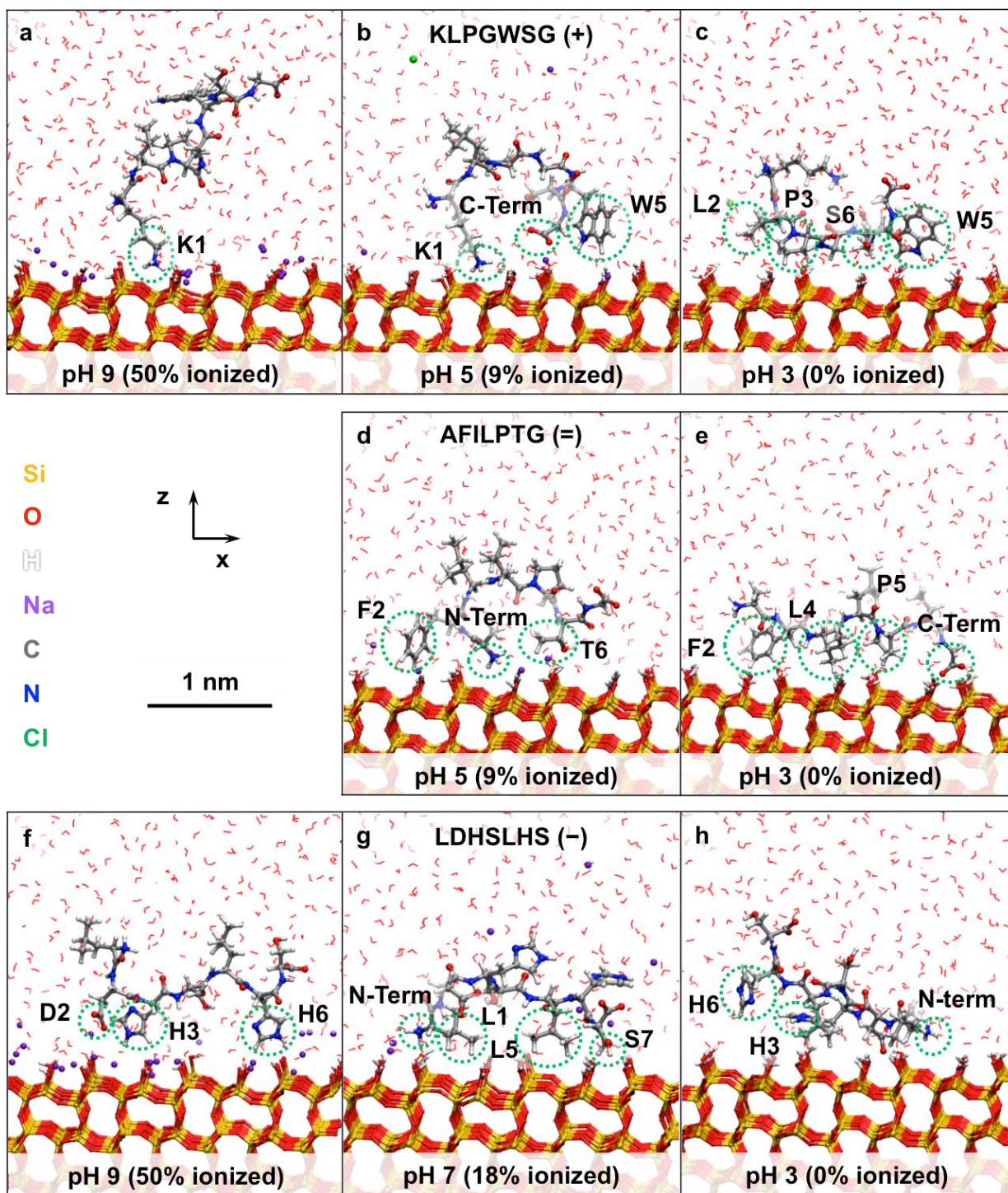


Figure 4. Selected conformation of three peptides of different charge on Q³ silica surfaces for a series of pH values according to simulation. The surfaces represent silica particles of 82 nm size with 4.7 SiO(H, Na) groups per nm² and variable ionization. (a-c) The positively charged peptide

KLPGWSG, (d,e) the overall neutral peptide AFILPTG, (f-h) the negatively charged peptide LDHSLHS. Amino acids with significant surface interactions are highlighted. Close contact with the surface as shown occurs between >90% (a) and 20% (f) of time depending on affinity.

Table 3. Adsorption strength of peptides bound to Q³ silica surfaces at different pH values, characterized by the percentage of simulation time in close contact with the surface, i.e., <3 Å vertical distance from the superficial layer of silanol oxygen atoms. Amino acids are ranked in the order of proximity to the surface with the closest first. Statistical uncertainties in time averages are ±5%.

Peptide	pH~3 (0% ionized)		pH~5 (9% ionized)		pH~7 (18% ionized)		pH>8.5 (50% ionized)	
	Time	Closest residues	Time	Closest	Time	Closest	Time	Closest
	%		%	residues	%	residues	%	residues
KLPGWSG (+)	30	W5, K1, N-terminal, P3, S6 (hydrophobic interactions dominate at lower ionization)	65	N-term, K1>>C term >L2, W5, P3	75	N-term, K1 >>C-term, S6>>P3, W5, L2	90	N-term, K1>>C- term> S6, W5
AFILPTG (=)	50	N-term, C-term, T6, F2, L4, I3, P5	50	N-term> C- term, T6, F2, L4, I3, P5	40	N-term> C- term, T6, F2, L4, I3	30	N-term> C- term, T6> F2> L4, I3
LDHSLHS (-)	60	N-term, C-term, S7, D2, S4, H3, H6, L1, L5	40	N-term, C- term, S7, D2, S4, H3 H6, L1, L5	40	N-term, C- term > S7, D2, S4, H3, H6, L1, L5	20	N-term, C- term > S7, D2, S4, H3, H6, L1, L5

In summary, molecular dynamics simulation with the new silica force field predicts peptide adsorption as a function of pH in remarkable correlation with experiment, and contributions to binding can be traced in atomic detail. Ion pairing, hydrogen bonds, and hydrophobic interactions, as well as conformation effects (especially for longer peptides and proteins) contribute to selective binding.⁹ Electrostatic and polar interactions are thereby stronger than hydrophobic interactions. Hydrophobic interactions become significant at lower degree of surface ionization and involve many binding sites throughout the peptide chain, driven by the separation of hydrophobic groups from the aqueous phase onto the surface. The contribution of each binding mode can be quantified and visualized for specific surface conditions and biomolecules. Changes in proton distribution on the peptides such as across L1, D3, H3, H6, and S7 residues of LDHSLHS are also essential to understand selective adsorption as a function of pH. Future studies may also explore simulations with multiple adsorbed peptides corresponding to higher initial peptide concentration.

3.2. Specific Peptide Adsorption as a Function of Silica Nanoparticle Size. In this section, it is shown how the same approach can be applied to understand specific peptide binding to silica particles of variable size (Figure 1). Silica nanoparticles of different synthetic origin are generally distinguishable by differences in surface chemistry and topology, and in turn attract highly dissimilar peptides.^{9, 10, 37, 42, 74} A common example is Stöber-type silica nanoparticles of different size that are produced using different amounts of ammonia to hydrolyze precursors, and in turn attract peptides of less than 20% sequence similarity at the same pH value.⁹ ζ -potential measurements show that larger silica nanoparticles exhibit more surface ionization and a lower point of zero charge (Figures 1 and S1), thus attracting peptides of higher positive charge (higher isoelectric point pI).^{9, 37, 42} *Qualitatively*, this relation was previously verified by molecular

simulations, which showed that combinatorially selected peptides binding to 82 nm particles (pep 1, KSLSRHDHIHHH, pI 8.8) were less attracted to 450 nm particles, and combinatorially selected peptides binding to 450 nm particles (pep4, MHRSDLMSAAVR, pI 9.4) were less attracted to 82 nm particles.⁹ The surfaces were then approximated as ionized Q³ environments for 82 nm particles and as ionized Q² environments for 450 nm particles, respectively, using the PCFF-SILICA force field (please refer to Table S1 for details of the surface chemistry of silica particles of different chemistry and size).³⁷

Recent further characterization by TEM, SEM, BET, BJH, TGA, XPS, and ζ -potential measurements quantified size-dependent differences in surface chemistry, including the area density of silanol groups (silanol number), the degree of ionization, surface morphology, and porosity (Figure 5a, see details in section S2).⁴² Therefore, silica nanoparticles of 28, 82, and 210 nm size and the same set of peptides as above (Table 1) were chosen to evaluate the influence of particle size on specific peptide adsorption at a constant pH value of 7.4 (Figure 5b). *Quantitative* affinity predictions by molecular dynamics simulations are in good agreement with measurements (Figure 5c), although differences for poorly defined surfaces of 28 nm particles are also noted.

A critical aspect hereby is the use of realistic surface models. TEM and SEM measurements show the irregular, “spongy” structure of 28 nm nanoparticles in contrast to the well-developed spherical geometry of larger particles (Figure 1a-d). Due to the lack of specific information, regular surfaces were nevertheless assumed for simplicity. For 82 nm and 210 nm particles with some mesoporosity or negligible porosity, respectively, regular surface topography on the 5 nm scale is a good approximation. Differences in total SiOH area density and surface acidity according to TGA and ζ -potential measurements are significant (Figure 5a)⁴² and were

appropriately matched to the area density of silanol groups and ionization in the surface models (Figure 2). The small and medium size particles of 18 nm and 82 nm size were accordingly represented by regular Q³ surfaces with a silanol density of 4.7 groups per nm² with 9% and 18% ionization, respectively, consistent with data about the pzc and surface titration (Table S1).^{9, 38-41} The nanoparticles of 210 nm size were represented by a mixed Q²/Q³ surface with a silanol density of 6.5 groups per nm² and 20% ionization, accounting for higher silanol density and lower pzc. The cation density per unit area was thus 54% higher in 210 nm particles than in 82 nm particles. Nanoparticles of 500 nm size could be represented by the same mixed Q²/Q³ surface with ~30% ionization (2.0 SiO⁻ Na⁺ groups per nm²), which further increases peptide adsorption without a significant change in ζ -potential.³⁷

Details of the adsorption mechanism of the peptides as a function of particle size can be inferred from the percentage of time in contact with the surface (Figure 5), conformations in contact with the surface (Figure 6), and the ranked list of proximity of individual residues (Table S3). Adsorption of all three peptides increased towards larger particles, i.e., towards higher surface ionization at pH ~7.4. The variable surface charge of Stöber-type silica particles of different size tunes the adsorption mechanism and selective binding of biomolecules similar to the effect of variable pH (Figure 2).

On the surfaces attributed to the largest particles (210 nm), binding is dominated by electrostatic interactions (Figure 6a, d, g and Table S3). Also, the contribution by hydrogen bonds was significant due to the high total silanol density and surface acidity of the silica surfaces. N-termini of all peptides and the positively charged ammonium group of K1 in KLPGWSG were the primary functional groups that account for peptide adsorption. Hydrogen bonds also involved C-termini in all peptides for significant percentages of time, as well as S6 in

KLPGWSG, T6 in AFILPTG, and S7, D2, S4, H3, and H6 in LDHSLHS. Weaker, intermittent hydrophobic interactions were also observed as a result of peptide exclusion from the solution towards the surface, particularly for the AFILPTG peptide with hydrophobic moieties in side chains of F2, I3, L4, P5, and T6 residues. Notably, even the negatively charged peptide LDHSLHS was somewhat drawn to the surface, and hydrophobic groups in all peptides were comparatively distant from the surface due to strong surface-water interactions.

On the surfaces attributed to smaller 82 nm particles, represented by pure Q³ models with 4.7 SiO(H, Na) and 18% ionization, the significance of ion pairing and hydrogen bonds decreased, resulting in lower affinity of all three peptides (Figure 6b, e, h and Table S3). The most attracted residues are similar to those seen for 210 nm particles, however, the percentage of time being anchored and exposed to the surface was reduced. Amongst the three peptides, the adsorption of AFILPTG on the surface of 82 nm particles had the sharpest decrease in binding from ~70% on to ~40% of time in close contact, which was mainly associated with the decrease in attraction of the peptide N-terminus.

On silica surfaces representing 28 nm nanoparticles, the adsorption of peptide KLPGWSG decreased somewhat further due to less electrostatic attractions. Adsorption of AFILPTG occurred intermittently for ~50% of simulation time primarily mediated by hydrophobic groups, and proximity of LDHSLHS was observed ~40% of simulation time through hydrogen bonds (Figure 6c, f, i). The adsorption mechanism on the surfaces of smaller silica particles involved less ion pairing, less hydrogen bonds, and increasingly hydrophobic interactions, similar to adsorption at low pH.

As mentioned above, the experimentally measured adsorption for the 28 nm samples is substantially lower than the affinity predicted by molecular dynamics simulation on idealized

regular surfaces (Figure 5b,c). Thereby, the relative trend in peptide attraction is still consistent between measurements and simulation. The authors believe that structural irregularities (Figure 1a) make much of the internal, nitrogen-accessible surface area in BET measurements unavailable to peptide adsorption, which was reported relative to the BET area in measurements (Figure 5, Figure S3, section S2). Previous studies also report poor definition and plasticity, as well as incomplete dissociation of organic precursor groups for Stöber-type silica particles smaller than 50 nm.⁷⁵ The disproportionately weak adsorption of peptides in experiment (Figure S3) may thus be related to overestimated surface area and partly to the presence of some residual hydrophobic organic groups on the silica surface (see more details in section S4). Certainly, more work is needed to consolidate poorly defined silica nanostructures with representative models.

In summary, computational predictions of biomolecular binding as a function of particle size correlate well with measurements. Close correspondence of true surface chemistry and morphology to the representation in models is thereby essential. The demonstrated sensitivity enables binding predictions for numerous existing and novel silica morphologies, as well as the elucidation of irregular silica structural models consistent with experimental information on structure and binding that often remains incomplete.

a

Information from experiment					Model	
Particle size (nm)	Porosity	BET surface area (m ² /g)	SiO(H, Na) (nm ⁻²)	pzc	SiO(H, Na) (nm ⁻²)	Ionization (%)
210	Non-porous	21	6.5 (1)	2.2 (2)	6.5 (Q ² /Q ³)	20
82	Mesoporous	65	4.5 (1)	2.4 (2)	4.7 (Q ³ np)	18
28	Irregular, porous	243	4.5 (1)	3.1 (2)	4.7 (Q ³ np)	9

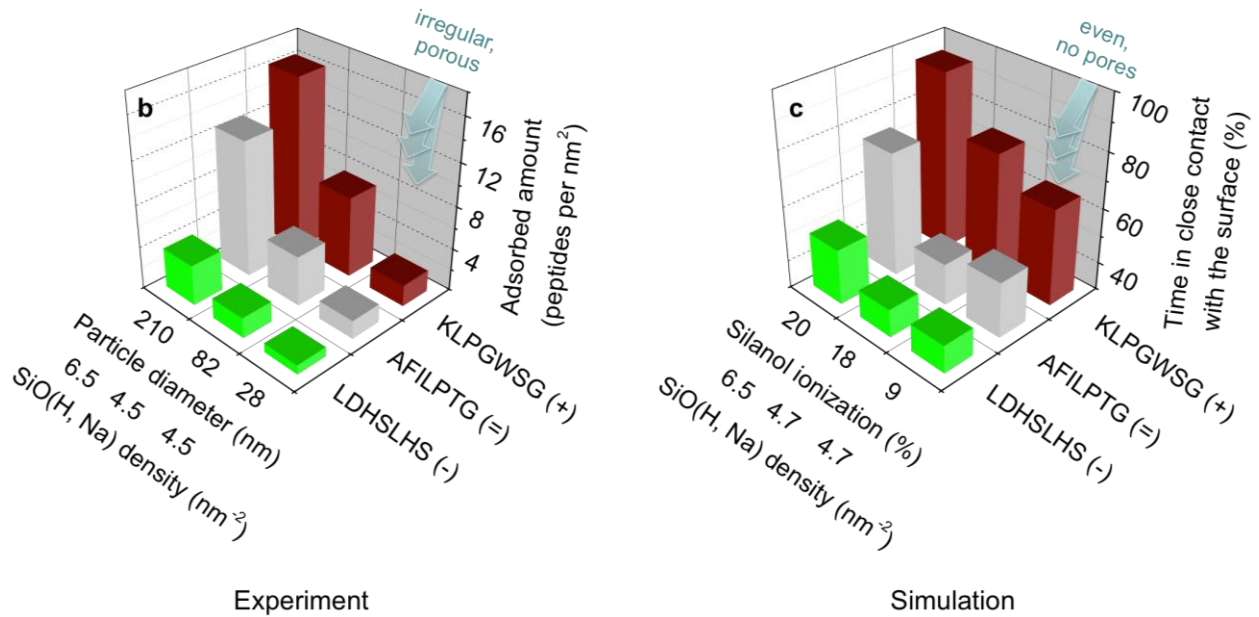


Figure 5. Adsorption spongy of peptides on silica nanoparticles of different size with particular surface features in experiment and simulation at pH = 7.4. (a) Nanoparticle characteristics (from ref. ⁴²) and corresponding model assumptions (np=non-porous). (b) Adsorbed amount of three peptides of different charge per BET surface area in experiment at 1 mM initial peptide concentration. (c) Percentage of time that peptides are in direct contact with the surface (<3 Å) in the simulation. The agreement is good, and the high impact of irregularity on adsorption is seen

for the 28 nm particles (poor particle definition in experiment b versus ideal regular surfaces in simulation c).

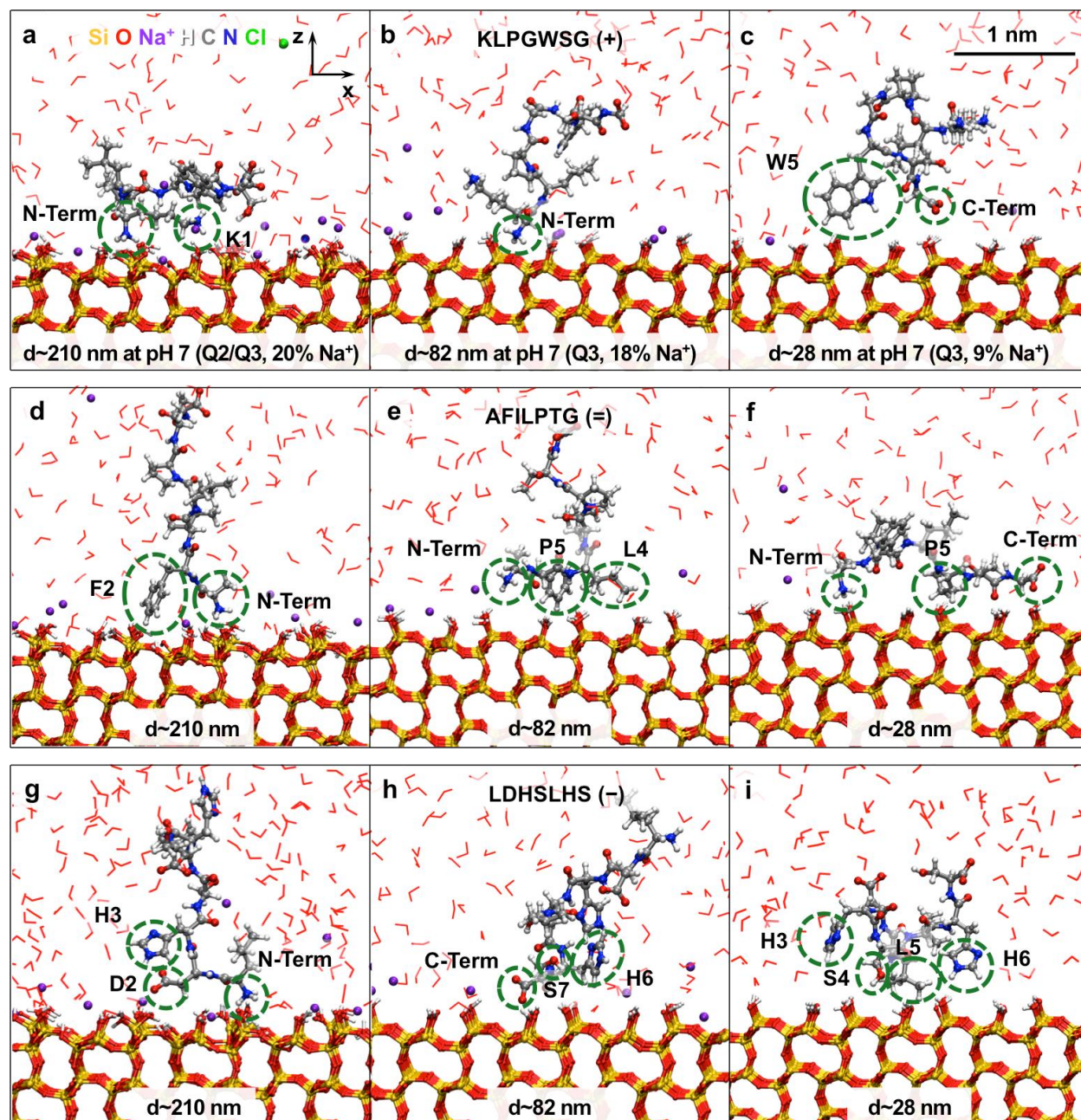


Figure 6. Selected conformations of three peptides of different charge on silica surfaces representing nanoparticles of 210 nm, 82 nm, and 28 nm sizes at pH ~ 7. (a-c) The positively charged peptide KLPGWSG, (d-f) the neutral peptide AFILPTG, (g-i) the negatively charged

peptide LDHSLHS. Amino acids with significant surface interaction are highlighted. The actual percentage of time in close contact with the surface varies between 90% (a) and 40% (e, h, and i) depending on affinity (see Table S3).

4. Conclusions

In conclusion, specific silica surface models of different degree of ionization were employed to study the adsorption of various peptides as a function of pH and particle size. Data from adsorption isotherms and from molecular simulation were found to be in very good correlation, showing that the INTERFACE-CHARMM force field and a surface model database^{26, 37} are suitable to predict selective adsorption in atomic resolution.

The results also reiterate the mechanism of adsorption and rationally explain the contribution of different factors in the context of the surface chemistry and charge states of silica and peptides. The contributions to selective adsorption involve ion pairing, hydrogen bonds, conformation effects, and hydrophobic interactions. A higher pH value in the solution results in higher negative charge density on the silica surface and shifts adsorption towards positively charged peptides, diminishing the attraction of negatively charged peptides, the influence of hydrogen bonds and hydrophobic interactions. pH had little effect on neutral peptides, which were more weakly bound by hydrogen bonds and hydrophobic interactions. At lower pH, binding differentials between all peptides diminish and hydrophobic residues increasingly interact with the surface. Binding of the same peptides to three batches of silica nanoparticles of different diameters showed stronger adsorption on larger particles with higher surface silanol density (Q^2/Q^3 environments), surface ionization, and absence of porosity. Weaker hydrophobic interactions on less ionic surfaces originate from the exclusion of peptides from the aqueous

phase to minimize disruptions of the network of hydrogen bonds. The different contributions to binding are tunable in customized proportions and can be evaluated by molecular dynamics simulation. Poor definition and “sponginess” of small (28 nm silica) nanoparticles showed much reduced peptide attraction, in part related to limited accessibility of the BET surface area.

While the force field accurately predicts binding of biomolecules for the chosen conditions, the representation of silica surface structure in the models must be handled with care. The feasibility of predictive simulations can be applied to a wide range of surface chemistry and topology, multiplied by a huge number of specific biomolecules and adsorbents, to engineer silica materials for desired performance at the atomic scale. In combination with new synthesis and characterization methods, computations can reduce the time spent on trial-and-error based chemistry. The models can be applied to screen the binding and release of drug molecules to customized silica nanostructures, evaluate silica nanoparticle interactions with specific receptors on cell surfaces, track the adsorption of gases in silica glasses and zeolites (using complementary parameters for aluminosilicates),²⁶ and assess the self-assembly of silica nanostructures, polymer and hydrogel composites at given pH, ionic concentration, and temperature.

Acknowledgement

We acknowledge support from the Air Force Research Laboratory, UES, Inc., the Air Force Office of Scientific Research (F. S. E. and H. H. via FA8650-09-D-5037, C. C. P. via FA9550-10-1-0024 and FA9550-13-1-0040), the National Science Foundation (DMR-0955071), the University of Akron, and the Ohio Supercomputing Center for the allocation of computational resources.

Supporting Information Available: Complete details of computational methods, experimental methods, experimental data for model validation, additional discussion of specific peptide binding, as well as supporting Figures and Tables. This information is available free of charge at <http://pubs.acs.org/>.

References

1. Hoffmann, F.; Cornelius, M.; Morell, J.; Froba, M. *Angew. Chem. Int. Ed.* **2006**, *45*, 3216-3251.
2. Iler, R. K., *The Chemistry of Silica: Solubility, Polymerization, Colloid and Surface Properties, and Biochemistry*. John Wiley & Sons: New York, 1979.
3. Slowing, II; Trewyn, B. G.; Giri, S.; Lin, V. S. Y. *Adv. Funct. Mater.* **2007**, *17*, 1225-1236.
4. Mackowiak, S. A.; Schmidt, A.; Weiss, V.; Argyo, C.; von Schirnding, C.; Bein, T.; Bräuchle, C. *Nano Lett.* **2013**, *13*, 2576-2583.
5. Hildebrand, M. *Chem. Rev.* **2008**, *108*, 4855-4874.
6. Kaehr, B.; Townson, J. L.; Kalinich, R. M.; Awad, Y. H.; Swartzentruber, B. S.; Dunphy, D. R.; Brinker, C. J. *Proc. Natl. Acad. Sci. U.S.A.* **2012**, *109*, 17336-17341.
7. Kröger, N.; Lorenz, S.; Brunner, E.; Sumper, M. *Science* **2002**, *298*, 584-586.
8. Patwardhan, S. V. *Chem. Comm.* **2011**, *47*, 7567-7582.
9. Patwardhan, S. V.; Emami, F. S.; Berry, R. J.; Jones, S. E.; Naik, R. R.; Deschaume, O.; Heinz, H.; Perry, C. C. *J. Am. Chem. Soc.* **2012**, *134*, 6244-6256.
10. Puddu, V.; Perry, C. C. *ACS Nano* **2012**, *6*, 6356-6363.
11. Sarthou, G.; Timmermans, K. R.; Blain, S.; Treguer, P. *J. Sea Res.* **2005**, *53*, 25-42.

12. Sumper, M.; Brunner, E. *Adv. Funct. Mater.* **2006**, 16, 17-26.
13. Cha, J. N.; Stucky, G. D.; Morse, D. E.; Deming, T. J. *Nature* **2000**, 403, 289-292.
14. Kröger, N.; Deutzmann, R.; Sumper, M. *Science* **1999**, 286, 1129-1132.
15. Muller, W. E. G.; Schroder, H. C.; Burghard, Z.; Pisignano, D.; Wang, X. H. *Chem. Eur. J.* **2013**, 19, 5790-5804.
16. Patwardhan, S. V.; Clarson, S. J.; Perry, C. C. *Chem. Commun.* **2005**, 1113-1121.
17. Perry, C. C.; Patwardhan, S. V.; Deschaume, O. *Biochem. Soc. Trans.* **2009**, 37, 687-691.
18. Rimola, A.; Costa, D.; Sodupe, M.; Lambert, J.-F.; Ugliengo, P. *Chem. Rev.* **2013**, 113, 4216-4313.
19. Stober, W.; Fink, A.; Bohn, E. *J. Colloid Interface Sci.* **1968**, 26, 62-69.
20. Vigil, G.; Xu, Z. H.; Steinberg, S.; Israelachvili, J. *J. Colloid Interface Sci.* **1994**, 165, 367-385.
21. Coppage, R.; Slocik, J. M.; Ramezani-Dakhel, H.; Bedford, N. M.; Heinz, H.; Naik, R. R.; Knecht, M. R. *J. Am. Chem. Soc.* **2013**, 135, 11048-11054.
22. Feng, J.; Pandey, R. B.; Berry, R. J.; Farmer, B. L.; Naik, R. R.; Heinz, H. *Soft Matter* **2011**, 7, 2113-2120.
23. Heinz, H. *Clay Miner.* **2012**, 47, 205-230.
24. Heinz, H.; Castelijns, H. J.; Suter, U. W. *J. Am. Chem. Soc.* **2003**, 125, 9500-9510.
25. Heinz, H.; Koerner, H.; Anderson, K. L.; Vaia, R. A.; Farmer, B. L. *Chem. Mater.* **2005**, 17, 5658-5669.
26. Heinz, H.; Lin, T.-J.; Mishra, R. K.; Emami, F. S. *Langmuir* **2013**, 29, 1754-1765.
27. Heinz, H.; Suter, U. W. *J. Phys. Chem. B* **2004**, 108, 18341-18352.
28. Heinz, H.; Suter, U. W.; Leontidis, E. *J. Am. Chem. Soc.* **2001**, 123, 11229-11236.

29. Mishra, R. K.; Flatt, R. J.; Heinz, H. *J. Phys. Chem. C* **2013**, 117, 10417-10432.
30. Ruan, L.; Ramezani-Dakhel, H.; Chiu, C.-Y.; Zhu, E.; Li, Y.; Heinz, H.; Huang, Y. *Nano Lett.* **2013**, 13, 840-846.
31. Ugliengo, P.; Sodupe, M.; Musso, F.; Bush, I. J.; Orlando, R.; Dovesi, R. *Adv. Mater.* **2008**, 20, 4579-4583.
32. Schneider, J.; Ciacchi, L. C. *J. Am. Chem. Soc.* **2012**, 134, 2407-2413.
33. Wright, L. B.; Walsh, T. R. *Phys. Chem. Chem. Phys.* **2013**, 15, 4715-4726.
34. Calzolari, A.; Cicero, G.; Cavazzoni, C.; Di Felice, R.; Catellani, A.; Corni, S. *J. Am. Chem. Soc.* **2010**, 132, 4790-4795.
35. Heinz, H. *J. Phys.: Condens. Matter* **2014**, 26, 244105.
36. Liu, H.; Espe, M.; Modarelli, D. A.; Arias, E.; Moggio, I.; Ziolo, R. F.; Heinz, H. *J. Mater. Chem. A* **2014**, 2, 8705-8711.
37. Emami, F. S.; Puddu, V.; Berry, R. J.; Varshney, V.; Patwardhan, S. V.; Perry, C. C.; Heinz, H. *Chem. Mater.* **2014**, 26, 2647-2658.
38. Bolt, G. H. *J. Phys. Chem.* **1957**, 61, 1166-1169.
39. Tadros, T. F.; Lyklema, J. *J. Electroanal. Chem. Interfacial Electrochem.* **1968**, 17, 267-275.
40. Zerrouk, R.; Foissy, A.; Mercier, R.; Chevallier, Y.; Morawski, J.-C. *J. Colloid Interface Sci.* **1990**, 139, 20-29.
41. Sonnefeld, J. *J. Colloid Interface Sci.* **1996**, 183, 597-599.
42. Puddu, V.; Perry, C. C. *Langmuir* **2014**, 30, 227-233.
43. Sanders, M. J.; Leslie, M.; Catlow, C. R. A. *Journal of the Chemical Society-Chemical Communications* **1984**, 1271-1273.

44. van Beest, B. W. H.; Kramer, G. J. *Phys. Rev. Lett.* **1990**, 64, 1955-1958.
45. Hill, J. R.; Sauer, J. J. *Phys. Chem.* **1994**, 98, 1238-1244.
46. Cruz-Chu, E. R.; Aksimentiev, A.; Schulten, K. *J. Phys. Chem. B* **2006**, 110, 21497-21508.
47. Hassanali, A. A.; Singer, S. J. *J. Phys. Chem. B* **2007**, 111, 11181-11193.
48. Hassanali, A. A.; Zhang, H.; Knight, C.; Shin, Y. K.; Singer, S. J. *J. Chem. Theory Comput.* **2010**, 6, 3456-3471.
49. Lopes, P. E. M.; Murashov, V.; Tazi, M.; Demchuk, E.; MacKerell, A. D. *J. Phys. Chem. B* **2006**, 110, 2782-2792.
50. Butenuth, A.; Moras, G.; Schneider, J.; Koleini, M.; Köppen, S.; Meißner, R.; Wright, L. B.; Walsh, T. R.; Ciacchi, L. C. *Phys. Status Solidi B* **2012**, 249, 292-305.
51. Flikkema, E.; Bromley, S. T. *Chem. Phys. Lett.* **2003**, 378, 622-629.
52. Goumans, T. P.; Wander, A.; Brown, W. A.; Catlow, C. R. *Phys. Chem. Chem. Phys.* **2007**, 9, 2146-2152.
53. Skelton, A. A.; Fenter, P.; Kubicki, J. D.; Wesolowski, D. J.; Cummings, P. T. *J. Phys. Chem. C* **2011**, 115, 2076-2088.
54. Garofalini, S. H. *J. Chem. Phys.* **1982**, 76, 3189-3192.
55. Lockwood, G. K.; Garofalini, S. H. *J. Chem. Phys.* **2009**, 131, 074703.
56. Pedone, A.; Malavasi, G.; Menziani, M. C.; Segre, U.; Musso, F.; Corno, M.; Civalleri, B.; Ugliengo, P. *Chem. Mater.* **2008**, 20, 2522-2531.
57. Du, J.; Cormack, A. N. *J. Am. Ceram. Soc.* **2005**, 88, 2532-2539.
58. Gambino, G. L.; Lombardo, G. M.; Grassi, A.; Marletta, G. *J. Phys. Chem. B* **2004**, 108, 2600-2607.

59. Lobel, K. D.; West, J. K.; Hench, L. L. *J. Mater. Sci. Lett.* **1996**, 15, 648-650.
60. Rimola, A.; Civalleri, B.; Ugliengo, P. *Langmuir* **2008**, 24, 14027-14034.
61. Yang, J. J.; Meng, S.; Xu, L. F.; Wang, E. G. *Phys. Rev. B* **2005**, 71, 035413.
62. Oren, E. E.; Notman, R.; Kim, I. W.; Spencer, E. J.; Walsh, T. R.; Samudrala, R.; Tamerler, C.; Sarikaya, M. *Langmuir* **2010**, 26, 11003-11009.
63. Oren, E. E.; Tamerler, C.; Sahin, D.; Hnilova, M.; Seker, U. O. S.; Sarikaya, M.; Samudrala, R. *Bioinformatics* **2007**, 23, 2816-2822.
64. Argyris, D.; Cole, D. R.; Striolo, A. *Langmuir* **2009**, 25, 8025-8035.
65. Feng, J.; Slocik, J. M.; Sarikaya, M.; Naik, R. R.; Farmer, B. L.; Heinz, H. *Small* **2012**, 8, 1049-1059.
66. Fu, Y. T.; Heinz, H. *Chem. Mater.* **2010**, 22, 1595-1605.
67. Heinz, H.; Farmer, B. L.; Pandey, R. B.; Slocik, J. M.; Patnaik, S. S.; Pachter, R.; Naik, R. R. *J. Am. Chem. Soc.* **2009**, 131, 9704-9714.
68. Heinz, H.; Suter, U. W. *Angew. Chem. Int. Ed.* **2004**, 43, 2239-2243.
69. Heinz, H.; Vaia, R. A.; Koerner, H.; Farmer, B. L. *Chemistry of Materials* **2008**, 20, 6444-6456.
70. Heinz, H.; Vaia, R. A.; Krishnamoorti, R.; Farmer, B. L. *Chem. Mater.* **2007**, 19, 59-68.
71. Jha, K. C.; Liu, H.; Bockstaller, M. R.; Heinz, H. *J. Phys. Chem. C* **2013**, 117, 25969-25981.
72. Mishra, R. K.; Fernández-Carrasco, L.; Flatt, R. J.; Heinz, H. *Dalton Trans.* **2014**, 43, 10602-10616.
73. Heinz, H. *J. Comput. Chem.* **2010**, 31, 1564-1568.

74. Zhang, L.; D'Acunzi, M.; Kappl, M.; Imhof, A.; van Blaaderen, A.; Butt, H.-J.; Graf, R.; Vollmer, D. *Phys. Chem. Chem. Phys.* **2010**, 12, 15392-15398.
75. Costa, C. A. R.; Leite, C. A. P.; Galembeck, F. *J. Phys. Chem. B* **2003**, 107, 4747-4755.

TOC Illustration

